Equation (9) is used as the input of the proportional integral controller, and the output of the proportional integral controller is set to the estimated rotor angular velocity.

The PI controller gains can be expressed as follows:

$$K_P = \omega_g \sqrt{\frac{(tan\varphi_m)^2}{1+(tan\varphi_m)^2}} \tag{11}$$

$$K_i = \omega_g^2 \sqrt{\frac{1}{1+(tan\varphi_m)^2}} \tag{12}$$

where K_p, K_i, φ_m, and ω_g are the proportional gain, integral gain, phase margin, and the bandwidth, respectively.

Figure 3 shows a block diagram of a rotor position and speed estimator. The rotor position error is given by equations (9) and (10), and the rotor position error is compensated for rotor estimated speed by PI control. The estimated rotor position is obtained by integrating the estimated rotor speed. In general, in Eq. (10), the γδ –axis back-EMF is estimated using the output of the current controller.

In very low rotating speed, the estimated speed is very low, and it may make the estimated rotor position error θ_{err} become very large and the input of the position estimation PI controller become very large. This destabilizes the operation of the PI controller, which leads to poor start-up characteristics and, in some cases, causes start-up failures. Therefore, the speed estimation method shown in Figure 3 can be accurate in areas where the speed has increased by more than a certain degree. In order to avoid such a problem, a constant frequency pattern uses a method of starting the motor with open loop control at a low speed, and then switching to vector control when the speed increases over a certain speed. When this method is applied, it is difficult to adjust the acceleration/deceleration time because it needs to accelerate slowly in order to synchronize with the rotating magnetic field during start-up, and the current or voltage and frequency ratio of the open loop control must also be selected by trial and error. This is a long and probable mechanical and electrical problem during the tuning process.

To compensate this drawback at low speed, a simple dynamic compensator is added to improve the dynamic characteristics at low speed as shown in Fig. 4. By applying the fast compensator to the sensorless controller, it can be seen that the bandwidth at the low speed is increased. However, increasing the bandwidth through the compensator can lead to unstable operation due to inverter nonlinearity, which must be retuned through experimentation. The proposed method has the advantage that the motor constant is less dependent, and the algorithm is extremely simple compared to the existing methods.

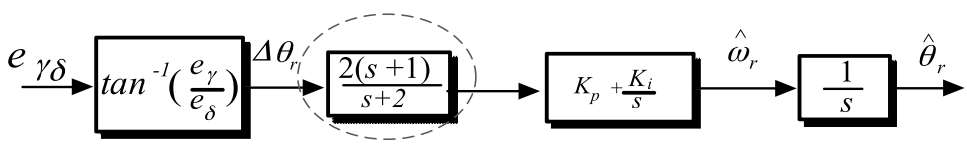

Figure 4. Block diagram of the proposed sensorless control with lead compensator.

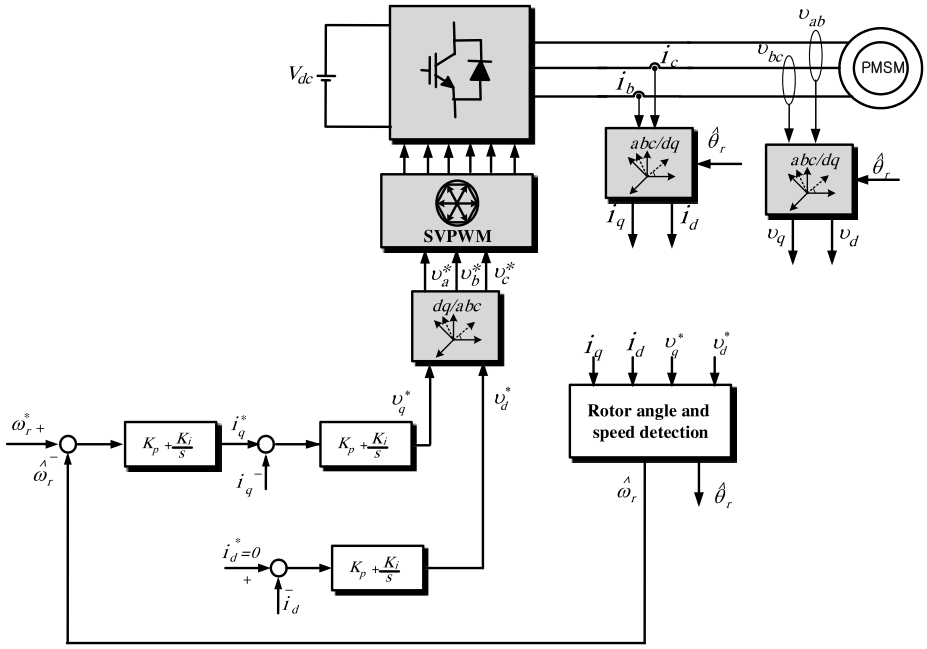

Figure 5. Block diagram overall control structure of constant frequency pattern method.

A complete block diagram of the proposed sensorless control of PMSM drive is shown in Fig. 5. The speed controller basically generates a current command so that the actual motor speed follows the speed command given from the outside. Therefore, the speed controller can fulfill its function only when the basic assumption that the torque coinciding with the current command is accurately output from the electric motor is established. This current command is fed to the current controller and used as the reference current of the current controller. At this time, the current controller operates fast enough so that the same current as the reference value is applied to the motor.

EXPERIMENTAL RESULTS

Figure 6 shows the complete control system built for the experiment to control permanent magnet synchronous motor. Basic configuration consists of 2.7 [kW] PMSM, 3 [kW] DC generator as a load used as wind simulator, inverter to supply electric power, and controller. The switching frequency of the PWM inverter was 10kHz, and the processor used was TMS320VC33-120MHz. The specifications of the PMSM are shown in Table 1 in the appendix.

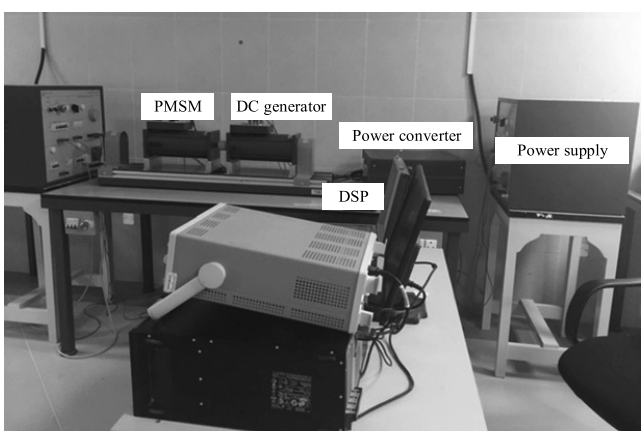

Figure 6. PMSM experimental setup.

Figure 7 shows the estimated speed, measured speed, and rotor position when the speed command of 400 [rpm] is given in steps. From the above, the estimated speed and measured speed show good speed response characteristics and estimated characteristics in the transient and steady state with respect to the step speed command.

Figure 8 shows the estimated speed and actual speed, estimated rotor position, and actual rotor position for the speed command of 400 [rpm]. In this figure, it can be seen that, in the transient state at the initial low speed, the dynamic characteristics are lowered because the bandwidth of the rotor position estimation PI controller is low. In the same principle, the estimated rotor position is also initially slow due to low bandwidth, but after a certain speed, the estimated bandwidth is also improved.

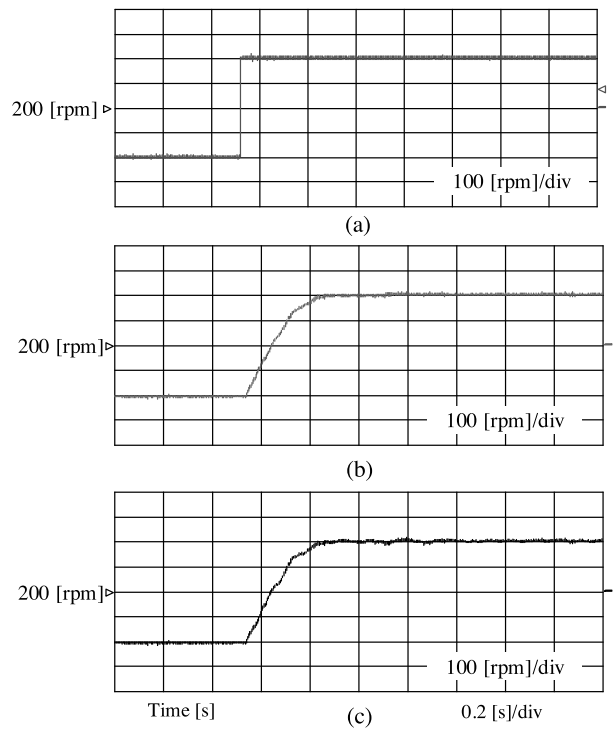

Figure 7. Estimated and measured speed/position with a step 400rpm command change.

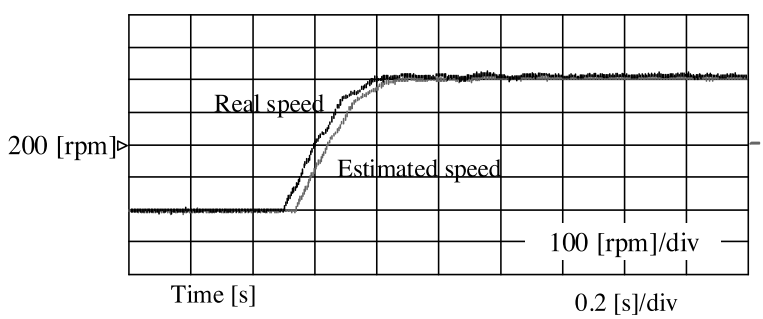

Figure 8. Estimated speed/position with a step 400rpm command change.

Figure 9 shows rotor position estimation characteristics at steady state for the speed command of 400 [rpm]. As can be seen from the figure, the rotor position error in the low speed region of 400 [rpm] is almost zero, which shows good position estimation characteristics.

Figure 10 shows the estimated and measured rotor speed when the speed command is changed to 500-600-500 [rpm]. As can be seen from the figure, even when the speed command is changed to 500-600-500 [rpm] in steps, it shows stable response characteristics and estimated characteristics.

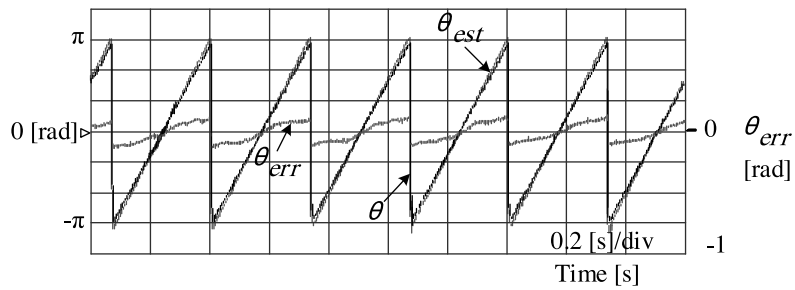

Figure 9. Responses of position estimation with 400[rpm] speed command (steady state).

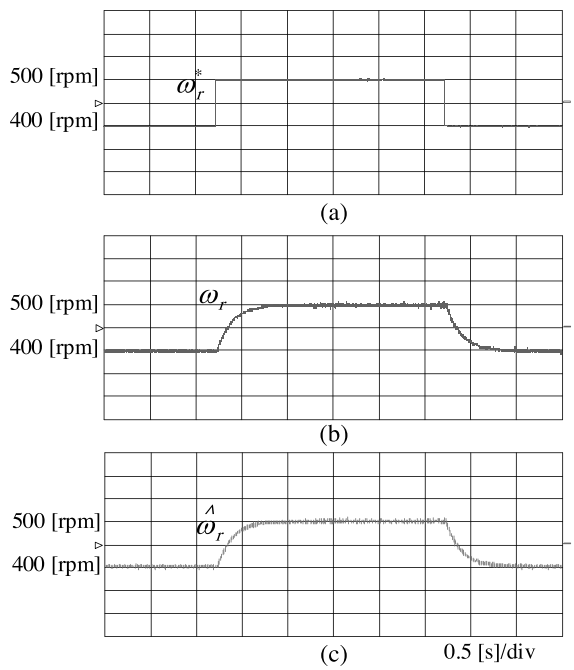

Figure 10. Responses of 400-500-400 [rpm] step speed command.

Figure 11 shows the performance of the speed controller at 800 rpm speed command. It is noticed that the speed is maintained at 800 rpm, and the q-axis current is well controlled with low harmonic content.

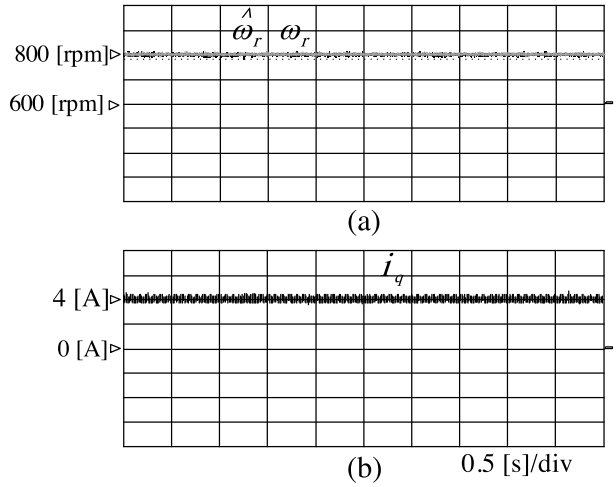

Figure 11. Steady-state responses of 800[r/min] speed command with full load test.

CONCLUSION

In this paper, a sensorless method that can be applied to high and low speed operation of PMSM such as turbo compressors and flywheels is proposed. Considering the error between the actual rotor position and the estimated position, the back emf is determined based on the estimated speed and position. A new rotating reference frame, namely, γδ-axis, is presented. The two components of EMF are then analyzed in the new coordinates and used to detect and control the motor speed. A lead error compensator is added to the detector to reduce the error in the starting and low speed conditions. By performing and experiments, we verified the superiority and feasibility of all the proposed algorithms and also showed that the sensorless PMSM controller for high performance control can be put into practical use.

ACKNOWLEDGMENT

The author would like to thank Deanship of Scientific Research at Majmaah University for supporting this work under Project Number No. (RG. 2019-19)

REFERENCES

Abo-Khalil, A.G. Berrouche, Y. Barhoumi, E.M. Baseer, A.M. Praveen, R.P. & Awan, A.B. 2016. A low-cost PMSG topology and control strategy for small-scale wind power generation systems. International Journal of Engineering Sciences & Research Technology, IJESRT, 585-592.

Baseer, A.M. Abo-Khalil, A.G. & Agora, S. 2015. Positioning and adjusting the frequencies of the rotor in permanent magnet synchronous machine to achieve high performance" International Journal of Applied Engineering Research, **10**(59): 379- 386.

Chan, T.F. Wang, W. Borsje, P. Wong, Y.K. & Ho, S.L. 2008. Sensorless permanent-magnet synchronous motor drive using a reduced-order rotor flux observer. IET Electric Power Applications, **2**: 88-98.

Fernandes, E.M. Oliveira, A.C. Vitorino, M.A. Dos Santos, E.C. & Santos, W. R.N. 2014. Speed Sensorless PMSM Motor Drive System Based on Four Switch Three-Phase Converter. In Proceedings of the 40th Annual Conference of the IEEE Industrial Electronics Society, Dallas, TX, USA.

Flieh, H. Slininger, T. Lorenz, R.D. & Totoki, E. 2018. Self-Sensing via Flux Injection with Servo Dynamics including a Smooth Transition to Back-EMF Tracking. In Proceedings of the 2018 IEEE Energy Conversion Congress and Exposition (ECCE), Portland, OR, USA: 1762-1769.

Janiszewski, D. 2012. Unscented Kalman Filter for sensorless PMSM drive with output filter fed by PWM converter. In Proceedings of the IECON 2012—38th Annual Conf. IEEE Industrial Electronics Society, Monteral, QC, Canada: 4660-4665.

Kivanc, O.C. & Ozturk, S.B. 2015. MATLAB Function Based Approach to FOC of PMSM Drive. In Proceedings of the IEEE European Modelling Symposium, Madrid, Spain.

Kwon, Y.C. Sul, S.K. Baloch, N.A. Murakami, S. & Morimoto S. 2016. Improved design of IPMSM for sensorless drive with absolute rotor position estimation capability. IEEE Transaction of Industrial Applications, **52**(2): 1441-1451.

Ma, Z. & Zhang, X. 2018. FPGA Implementation of Sensorless Sliding Mode Observer With a Novel Rotation Direction Detection for PMSM Drives. IEEE Access, **6**: 55528-55536.

Moujahed, M. Ben Azza, H. Jemli., M. & Boussak, M. 2013. Sensor-less direct torque control of permanent magnet synchronous motor drive using Extended Kalman filter," Electrical Engineering and Software Applications (ICEESA): 1-6.

Park, N.C. & Kim, S.H. 2014. Simple sensorless algorithm for interior permanent magnet synchronous motors based on high-frequency voltage injection method. IET Electric Power Applications, **8**(2): 68-75.

Shi, Y. Sun, K. Huang, L. & Li, Y. 2011. On-line identification of permanent magnet flux based on extended Kalman filter for IPMSM drive with position sensorless control. IEEE Transaction of Industrial Electronics, **59**(11): 4169-78.

Song, X. Fang, J. Han, B. & Zheng, S. 2016. Adaptive Compensation Method for High-Speed Surface PMSM Sensorless Drives of EMF-Based Position Estimation Error. IEEE Trans. Power Electron, **31**: 1438-49.

Wang, Z. Lu, Q. Ye, Y. Lu, K. & Fang, Y. 2012. Investigation of PMSM Back-EMF using Sensorless Control with Parameter Variations and Measurement Errors. Przeglad Elektrotechniczny, **88**: 182-186.

Wang, Y. Xu Y. & Zou, J. 2019. Sliding mode sensorless control of PMSM with inverter nonlinearity compensation. IEEE Trans. Power Electronics, **34**(10): 1450-1460.

Wisniewski, J. & Koczara, W. 2008. The sensorless rotor position identification and low speed operation of the axial flux permanent magnet motor controlled by the novel PIPCRM method. In Proceedings of the 2008 IEEE Power Electronics Specialists Conference, Rhodes, Greece: 1502-1507.

Xu, D. Wang, G. Zhang, G. & Yu, Y. 2018. A review of sensorless control methods for AC motor drives. CES Trans. Elect. Mach. Syst. **2**: 104-115.

Xu, W. Jiang Y. Mu, C. & Blaabjerg, F. 2019. Improved nonlinear flux observer-based second-order SOIFO for PMSM sensorless control. IEEE Trans. Power Electronics, **34**: 565-579.

APPENDICES

The specification of the PMSM used for test is listed in Table 1.

Table 1. Parameters of the PM synchronous machine.

Parameters	Value
Rated Power	2.7 [kW]
Rated speed	1200 [rpm]
Number of poles	6
Rated current	9.5 [A]
Stator resistance	0.5 [Ω]
d-axis inductance	3 [mH]
q-axis inductance	7 [mH]
Flux Linkage	0.175 [Wb]
Moment of inertia	$1.8X10^{-3}$ [$kg.m^2$]